JACS
JOURNAL OF THE AMERICAN CHEMICAL SOCIETY
pubs.acs.org/JACS
Article

Unveiling Janus Chemical Processes in Contact-Electro-Chemistry through Oxygen Reduction Reactions

Ting Gan,[▽] Zhe Yang,[▽] Shaoxin Li,[▽] Han Qian,[▽] Zhijian Li, Jiajin Liu, Puguang Peng, Jinbo Bai, Hanbin Liu,* Zhonglin Wang,* and Di Wei*

Cite This: J. Am. Chem. Soc. 2025, 147, 25407−25416

ABSTRACT: Oxygen reduction reaction (ORR), operating via four-electron (H_2O) or two-electron (H_2O_2) pathways, underpins critical processes in energy conversion and biological metabolism. Solid−liquid contact electrification enables 2e$^-$ ORR for both pollutant oxidation degradation and metal reduction without external metal catalysts. However, the criteria dictating oxidation versus reduction in such Janus contact-electro-chemistry (CE-Chemistry) systems remain unclear. This study systematically demonstrates that the redox selectivity in CE-Chemistry is controlled by the standard electrode potential (SEP) of the reactants, with a clear threshold distinguishing the oxidation and reduction pathways. Reduction of metal ions (e.g., $[AuCl_4]^-$, Pd^{2+}, $[PtCl_4]^{2-}$ Ag^+, Rh^{3+}, and Ir^{3+}) was achieved when their SEPs lie between the 2e$^-$ ORR (E^0 = 0.695 V vs NHE) and the 4e$^-$ ORR (E^0 = 1.229 V vs NHE). Conversely, SEPs below the 2e$^-$ ORR threshold favored oxidation (e.g., ferrocyanide). For the first time, methanol-to-formaldehyde oxidation was achieved in both aqueous and nonaqueous CE-Chemistry. Remarkably, the formaldehyde production rate in dimethyl sulfoxide was 25 times higher than in aqueous systems, which has already surpassed some photocatalytic processes. This study provides a comprehensive mechanistic framework for CE-Chemistry, highlighting the pivotal role of SEPs in regulating its Janus redox properties and the tunable radical reactivity in nonaqueous environments.

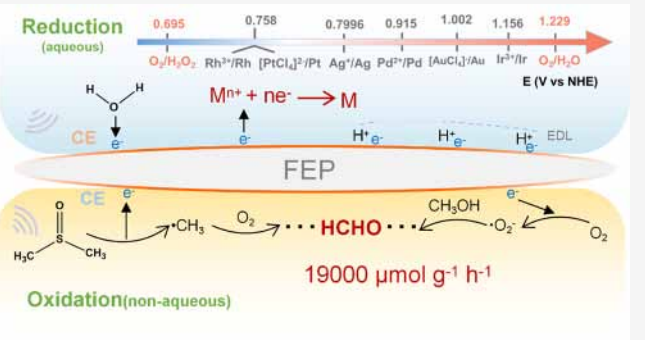

INTRODUCTION

In biological systems, ORR is an essential reaction in the respiratory chain,[1,2] where oxygen is progressively reduced through four-electron (4e$^-$) transfer chains to generate H_2O and sustain energy acquisition. In signaling and antioxidant processes, hydrogen peroxide (H_2O_2), as a key intermediate, is produced through a two-electron (2e$^-$) transfer process,[3] potentially linking it to the origin of life.[4] Remarkably, H_2O_2 generation extends beyond intracellular processes, spontaneously occurring at multiphase interfaces in nature through 2e$^-$ transfer ORR. For example, Zare's group revealed that H_2O_2 was produced when water vapor condensed into microdroplets on a low-temperature substrate, occurring without the need for metal catalysts or precursor chemicals.[5] Similarly, micron-sized droplets generated by atomizing water could drive H_2O_2 formation due to the intense electric fields at the water−air interface.[6,7]

In addition, solid−liquid interfaces driven by contact electrification (CE)-mediated electron transfer have been shown to facilitate H_2O_2 generation through water oxidation (WOR) and ORR.[8] Notably, Andy et al.[9] achieved a kinetic rate of 58.87 mmol g^{-1} h^{-1} for H_2O_2 generation at the CE of the water−solid interface, significantly surpassing rates observed in piezoelectric and photocatalytic systems. This approach was first introduced as contact-electro-catalysis (CEC) by Wang et al.[10] in 2022, utilizing electron transfer induced by CE to trigger subsequent radical generation and catalytic processes. CEC has attracted significant attention for its versatility, nonmetal catalysis, and broad range of applications,[11] including the degradation of methyl orange,[12,13] cost-effective H_2O_2 synthesis,[8,9] and the sustainable recovery of metallic materials from discarded lithium-ion batteries.[14] Recently, Wei's group expanded the scope of CEC to contact-electro-chemistry (CE-Chemistry), enabling diverse chemical processes such as redox reactions, polymerization, and fluorescence generation through electron transfer induced by CE.[15,16] However, many studies have primarily focused on partial reactions, where specific reactants undergo either oxidation or reduction without addressing the fundamental

Received: March 25, 2025
Revised: June 30, 2025
Accepted: July 1, 2025
Published: July 11, 2025

https://doi.org/10.1021/jacs.5c05124
J. Am. Chem. Soc. 2025, 147, 25407−25416

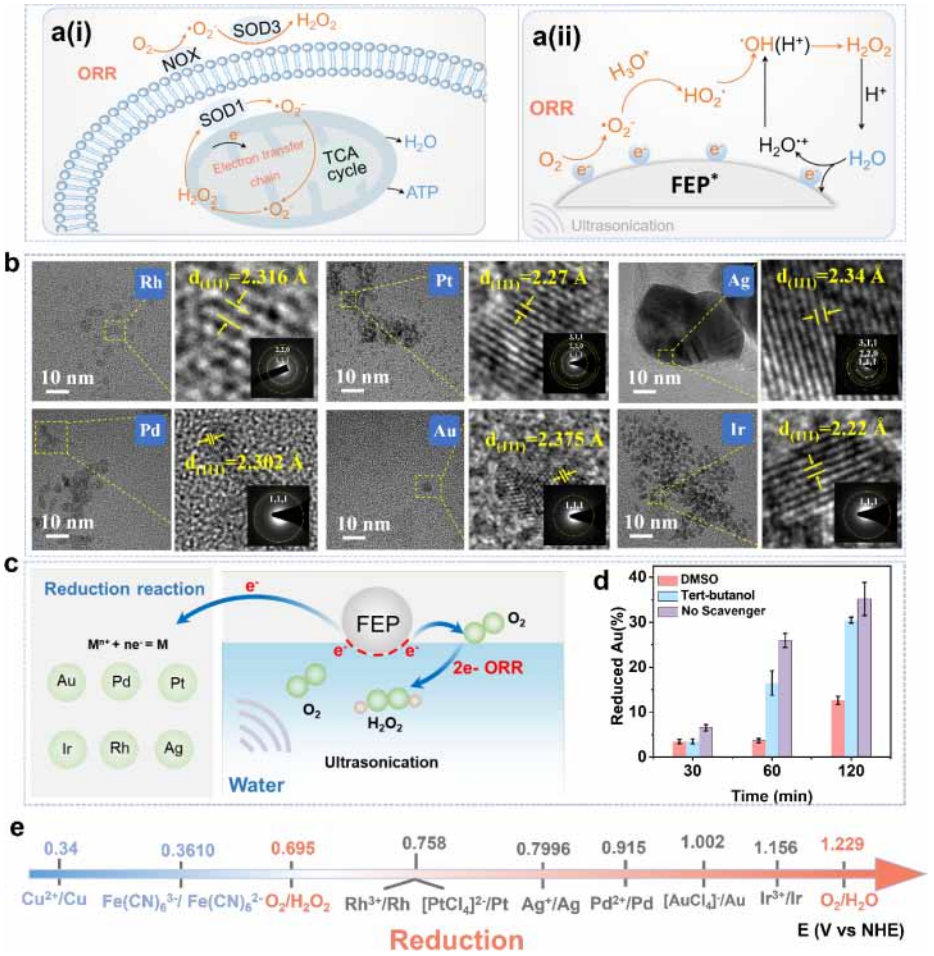

Figure 1. Janus characteristics of CE-Chemistry in aqueous systems. Redox reactions involved in organisms (a(i)) and FEP/water interfaces (a(ii)). (b) HRTEM and SAED diagrams corresponding to different metal ions. (c) Schematic of the reaction mechanism for metal ion reduction by CE-Chemistry. (d) Evolution of Au concentration in conditions of various radical scavengers. DMSO and *tert*-butanol were used as scavengers for electrons and •OH radicals, respectively. (e) SEPs of various metal ion reductions in the CE-Chemistry system.

principles underlying the Janus nature of CE-Chemistry. This lack of clarity on when oxidation or reduction occurs within the same system leaves the mechanistic understanding incomplete.

This study systematically explored redox reactions driven by CE in ultrasound-assisted CE-Chemistry systems, highlighting the pivotal role of the ORR in regulating the Janus nature of aqueous CE-Chemistry. Analysis of standard electrode potentials (SEPs) revealed that the reduction potentials of all aforementioned metal ions fall within the range defined by the $2e^-$ ORR (E^0 = 0.695 V vs NHE) and the $4e^-$ ORR (E^0 = 1.229 V vs NHE). Notably, reductions such as Cu^{2+} (E^0 = 0.34 V vs NHE) and $[Fe(CN)_6]^{3-}$) (E^0 = 0.361 V vs NHE) were undetectable when SEPs fell below 0.695 V, whereas the oxidation of potassium ferrocyanide ($K_2[Fe(CN)_6]$) to potassium ferricyanide ($K_3[Fe(CN)_6]$) was observed. These findings established the critical role of SEPs for the $2e^-$ and $4e^-$ ORR in dictating redox reaction directions in CE-Chemistry systems. In addition, for the first time, the oxidation reaction of methanol (CH_3OH) to formaldehyde (HCHO) has been achieved in both aqueous and nonaqueous CE-Chemistry systems. The amount of HCHO generated in the dimethyl sulfoxide (DMSO) system is 25 times higher than those obtained by CEC aqueous systems in existing literature,[17,18] which has already surpassed some photocatalytic processes.[19−23] This paper systematically investigates the relationship between the physical electron transfer capabilities, determined by the triboelectric series based on the electronegativity of the solid dielectric, and the electrochemical SEPs that govern chemical reactions at the solid−liquid CE interface. Additionally, this method might also reveal previously unrecognized pathways in CE-Chemistry, broadening our understanding of Janus characteristics.

■ RESULTS AND DISCUSSION

Reduction Reaction of Various Metal Ions via CE-Chemistry. ORR is a fundamental process ubiquitous in living organisms, playing a crucial role in cellular energy metabolism and respiration in aerobic systems. For example, in the mitochondria of eukaryotic cells, the ORR facilitates the reduction of oxygen to H_2O_2 or H_2O while driving ATP synthesis via electron transfer in the cellular respiration chain (Figure 1a(i)). Notably, a similar $2e^-$ ORR process facilitating H_2O_2 production was observed in the CE process, where oxygen acquires electrons during the solid−liquid CE process (Figure 1a(ii)), a redox phenomenon potentially linked to the origins of life.[4,24] The distinctive characteristics of the CE effect have attracted considerable attention for enabling the oxidative degradation of organic pollutants without the need for metal catalysts.[12,13] Meanwhile, under identical conditions,

https://doi.org/10.1021/jacs.5c05124
J. Am. Chem. Soc. 2025, 147, 25407−25416

the electrons transferred from the dielectric surface at the solid−liquid interface enable the reduction of specific metal ions.[14,25] Such a phenomenon revealed the Janus characteristics (both oxidation and reduction) intrinsic to the CE-Chemistry system. To systematically quantify these dual characteristics, various metal ions ($[AuCl_4]^-$, Pd^{2+}, $[PtCl_4]^{2-}$, Ag^+, Rh^{3+}, Ir^{3+}, Cu^{2+}, and $[Fe(CN)_6]^{3-}$) were selected to investigate their reduction behavior in CE-Chemistry.

As shown in Figure S1, ultrasonication (120 W, 40 kHz) was employed to induce contact-separation movements between fluorinated ethylenepropylene (FEP) and H_2O, facilitated by the cavitation bubble effect. Compared with the $KAuCl_4$ solution prior to ultrasonication, the UV−vis absorption peak at 307 nm significantly diminishes after ultrasonication in the presence of FEP, whereas no notable change was observed in the system subjected to ultrasonication alone without FEP (Figure S2). These results indicate that sonochemistry itself is insufficient to drive the observed redox reactions. Ultrasonication primarily facilitated frequent CE interactions between water and FEP in CE-Chemistry, enhancing electron transfer at the solid−liquid interface, a mechanism distinct from traditional sonochemistry.[26] As shown in Figure S3, a noticeable color change and precipitate formation were observed at the bottom of the beaker in the $KAuCl_4$ solution following the CE-Chemistry reaction. High-resolution transmission electron microscopy (HRTEM) and selected area electron diffraction (SAED) were conducted to elucidate the structural characteristics of the solid precipitates resulting from the aqueous $KAuCl_4$ in the CE-Chemistry system. The *d*-spacing of the obtained solid precipitate is 2.375 Å, which is in close agreement with the standard card data for elemental gold (PDF# 04-0784),[25] corresponding to the (111) plane (Figure 1b). Moreover, energy-dispersive X-ray (EDX) analysis confirmed the presence of the gold element in the obtained particles (Figure S4). These results demonstrated that gold ions in solution were effectively reduced to solid particles of Au^0 in the CE-Chemistry system. In addition, the reduction products of Pd^{2+}, $[PtCl_4]^{2-}$, Ag^+, Rh^{3+}, and Ir^{3+} were tested and analyzed by the same characterization methods (Figures 1b and S4). The results showed that all of these metal ions were reduced to their metallic phases, including gold (Au), palladium (Pd), platinum (Pt), silver (Ag), rhodium (Rh), and iridium (Ir). The *d*-spacing data of each particle were obtained by HRTEM analysis, and the specific results are shown in Table S1.

The schematic description of the possible reaction mechanism for metal ion reduction by CE-Chemistry is shown in Figure 1c. First, H_2O underwent continuous electron transfer toward the FEP during the CE process, driven by the differing electronegativities of the materials. This process allowed the FEP surface to accumulate a large number of electrons, which provided favorable conditions for the reduction of metal ions. Scavengers were commonly employed to investigate the reaction mechanism of CE-Chemistry, as they selectively target and neutralize specific radicals or reactive intermediates.[12] In this study, DMSO, acting as an electron scavenger,[25] was found to be the most effective at inhibiting the reduction of $KAuCl_4$, compared to *tert*-butanol, a hydroxyl radical ($^{\bullet}OH$) scavenger, and the system without any scavenger (Figure 1d). This finding highlights the critical role of electron transfer in the reduction of metal ions within CE-Chemistry. However, it is important to note that the UV−vis spectra of $K_3[Fe(CN)_6]$ and $CuSO_4$ showed negligible changes before and after the CE-Chemistry reaction (Figure S5), indicating that their reductions were suppressed.

The reduction capability of metal ions is well understood through the SEP,[27] denoted as E^0. E^0 is a fundamental metric in electrochemistry, which quantifies the tendency of an element or compound to gain electrons and be reduced. The higher the value of the SEP, the more readily the element undergoes reduction, i.e., gains electrons. In this study, metal ions with higher SEPs ($E^0 > E^0$ (O_2, $2H^+/H_2O_2$) = 0.695 V vs NHE), such as Pd^{2+}, $[PtCl_4]^{2-}$, Ag^+, Rh^{3+}, and Ir^{3+}, were successfully reduced in CE-Chemistry. In contrast, reduction reactions for Cu^{2+} (E^0 (Cu^{2+}/Cu) = 0.34 V vs NHE) and $[Fe(CN)_6]^{3-}$ (E^0 ($[Fe(CN)_6]^{3-}$)/($[Fe(CN)_6]^{4-}$) = 0.361 V vs NHE) were undetectable. Therefore, it could be inferred that the reduction activity of the metal ions in CE-Chemistry might be linked to their positions in the SEP series and the electron transfer efficiency of the CE. Figure 1e presents the SEPs of various metal ions in the CE-Chemistry system. The reduction reactions of these metal ions occur between the $2e^-$ ORR (E^0 (O_2, $2H^+/H_2O_2$) = 0.695 V vs NHE) and the $4e^-$ ORR (E^0 (O_2, $2H^+/H_2O$) = 1.229 V vs NHE). Metal ions with SEPs below 0.695 V exhibited minimal propensity for reduction reactions. Besides, the oxidation of $[Fe(CN)_6]^{4-}$ to $[Fe(CN)_6]^{3-}$ was observed. As depicted in Figure S6, the UV−vis absorption intensity for $[Fe(CN)_6]^{3-}$, i.e., the oxidized $K_4[Fe(CN)_6]$ increased with prolonged ultrasonication, and the solution color transitioned from transparent to green after 3 h of ultrasonication. This phenomenon was attributed to the generation of radicals, such as $^{\bullet}OH$ and superoxide radicals ($^{\bullet}O_2^-$), in the solution when H_2O molecules lose electrons to FEP during the CE process, thereby oxidizing $K_4[Fe(CN)_6]$ to $K_3[Fe(CN)_6]$.[15]

Influence of Oxygen on the Reduction Reactions in CE-Chemistry. The ORR involves the reduction of oxygen by accepting electrons in the reaction system. The impact of oxygen on the reduction of metal ions in CE-Chemistry was investigated under aerobic (ambient air environment) and anaerobic conditions (purging Ar). As shown in Figure S7, under the same ultrasonic treatment time in the presence of FEP, the UV−vis absorption peak intensity of $[AuCl_4]^-$ solution in aerobic conditions was significantly higher than that in anaerobic conditions. The absorption peak of the $[AuCl_4]^-$ solution nearly vanished after 9 h of ultrasonication under anaerobic conditions, indicating the complete reduction of $[AuCl_4]^-$. In contrast, $[AuCl_4]^-$ failed to achieve complete reduction after 12 h of ultrasonic treatment under aerobic conditions due to the presence of the ORR reaction. To further investigate this competition, we conducted controlled experiments by varying the oxygen partial pressure through purging with different O_2/Ar volume ratios. As shown in Figure S8, increasing the partial pressure of O_2 leads to a systematic decrease in the yield of reduced Au from $[AuCl_4]^-$, confirming that O_2 intercepts a significant portion of interfacial electrons that would otherwise reduce $[AuCl_4]^-$. Although precise determination of reaction rate constants in CE-driven systems is hindered by the complex, dynamic, and heterogeneous nature of the solid−liquid interface, our semiquantitative analysis reveals that the reduction rate of $[AuCl_4]^-$ decreases by approximately 74% under O_2-saturated conditions compared to an Ar-saturated environment.

Moreover, this difference in the reduction of $[AuCl_4]^-$ via CE-Chemistry can be further demonstrated by the cyclic voltammetry (CV) measurement. Using glassy carbon as the

https://doi.org/10.1021/jacs.5c05124
J. Am. Chem. Soc. 2025, 147, 25407−25416

working electrode, a platinum plate as the counter electrode, and Ag/AgCl as the reference electrode, the CV curves of the $KAuCl_4$ solution were recorded under aerobic and anaerobic conditions. As shown in Figure S9, the results revealed that the reduction peak area under anaerobic conditions was significantly larger than that under aerobic conditions. This indicated that a greater amount of $[AuCl_4]^-$ was reduced in the anaerobic environment. To investigate the reduction kinetics of $KAuCl_4$ under anaerobic and aerobic conditions, we systematically tested the concentration of $KAuCl_4$ at different reaction time points. As shown in Figure S10, this reaction follows a first-order kinetic model, with reaction rate constants of 0.7457 h^{-1} and 0.0428 h^{-1} under anaerobic and aerobic conditions, respectively. In addition, chronoamperometry measurements were used to effectively evaluate the diffusion coefficient of the reaction. Figure S11 presents the linear relationship of the measured current I versus $t^{-1/2}$. The diffusion coefficient (D) was determined from the slope of the plots of I versus $t^{-1/2}$ to be 5.06×10^{-8} cm^2 s^{-1}.

In anaerobic conditions, the reduction efficiency of various metal ions, including $[AuCl_4]^-$, Pd^{2+}, $[PtCl_4]^{2-}$, Ag^+, Rh^{3+}, and Ir^{3+}, is enhanced (Figures 2a and S12). These results further

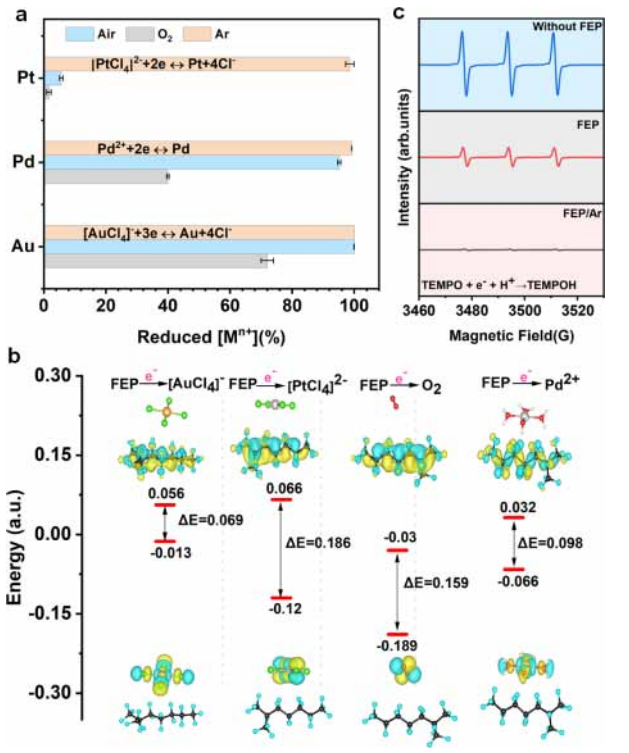

Figure 2. Influence of oxygen in CE-Chemistry. (a) The reduction amount of $[AuCl_4]^-$, Pd^{2+}, and $[PtCl_4]^{2-}$ in CE-Chemistry under aerobic and anaerobic conditions. (b) DFT simulations of electron transfer energy barriers in different metal ions. (c) Measured EPR spectra during the reduction of TEMPO to TEMPOH by ultrasonication of a TEMPO solution in different conditions.

indicate that under aerobic conditions, the presence of oxygen competes with metal ions for the available electrons on the surface of FEP generated by the CE process. This competition enhances the generation of H_2O_2, thereby diminishing the reduction efficiency. We conducted qualitative and quantitative tests on the generation of H_2O_2 in the metal ion reduction system. First, we used commercially available high-sensitivity H_2O_2 test strips for qualitative detection. As shown in Figure S13, when the $KAuCl_4$ solution after the CE-Chemistry reaction is dropped onto H_2O_2 test paper, the test paper turned blue, indicating the presence of H_2O_2 in the reaction system. We further quantitatively tested the concentration of H_2O_2 by the potassium titanium oxalate method. Specifically, H_2O_2 reacted with potassium titanium oxalate in a coordination reaction (Figure S14), forming a stable yellow complex with a characteristic UV−vis absorption peak around 400 nm, which is linearly related to the concentration of H_2O_2. Figure S15 shows the UV−vis spectra of H_2O_2 in the system before and after the CE-Chemistry reaction. Through the standard curve of potassium titanium oxalate (Figure S16), the concentration of H_2O_2 in the system was calculated to be 1.224 mM. This result indicates that the electron transfer at the solid−liquid interface in the CE-Chemistry system can simultaneously trigger the occurrence of oxidation and reduction reactions. This finding underscores the pivotal role of oxygen in modulating the electron transfer processes in CE-Chemistry systems, thereby influencing the Janus characteristics of the CE-Chemistry reactions.

Notably, the reduction of metal ions was inhibited to varying extents under aerobic conditions (air or O_2 purging) compared to anaerobic conditions (Ar purging), following the observed trend: $[PtCl_4]^{2-}$ > Pd^{2+} > $[AuCl_4]^-$ (Figure 2a). Specifically, the reduction of $[PtCl_4]^{2-}$ showed a pronounced disparity under aerobic conditions (~5% reduction) and under anaerobic conditions (~100% reduction). In addition, under anaerobic conditions, a substantial black precipitate formed in the $[PtCl_4]^{2-}$ solution after the CE-Chemistry reaction (Figure S17). HRTEM and EDX further confirmed that the obtained black precipitate was metallic Pt, demonstrating that the reduction reaction was successfully achieved by CE-Chemistry (Figure 1b). The apparent differences in the reduction of various metal ions under aerobic and anaerobic conditions might primarily stem from variations in the electron transfer energy barriers between the charged FEP surface and different metal ions. Density functional theory (DFT) simulations were employed to determine the electron transfer energy barriers (ΔE) between the lowest unoccupied molecular orbital (LUMO) of FEP and the highest occupied molecular orbital (HOMO) of metal ions for FEP-various metal ions ($[AuCl_4]^-$, Pd^{2+}, $[PtCl_4]^{2-}$) and FEP-O_2. Detailed computational parameters were provided in Simulation Methods. As illustrated by the simulated results in Figure 2b, the energy barriers between FEP and the metal ions followed the trend: FEP-$[AuCl_4]^-$ (0.069 au) < FEP-Pd^{2+} (0.098 au) < FEP-O_2 (0.159 au) < FEP-$[PtCl_4]^{2-}$ (0.186 au). This result indicated that $[AuCl_4]^-$ exhibited the lowest energy barrier for electron transfer from FEP under identical experimental conditions, thereby facilitating its preferential reduction to metallic Au. Under aerobic conditions, the preferential electron transfer from FEP to O_2, characterized by a lower energy barrier than that for FEP to $[PtCl_4]^{2-}$, competitively inhibits the reduction of $[PtCl_4]^{2-}$. This competitive electron transfer mechanism suppresses platinum deposition, leading to a reduced platinum yield in oxygen-rich environments.

To further elucidate the mechanism, the pH variations of the aqueous solution were monitored following ultrasonication in the absence and presence of FEP. As depicted in Figure S18, deionized (DI) water was neutral with a pH of around 7, while the pH of DI water containing FEP significantly decreased under the same ultrasonication conditions. The protons (H^+)

https://doi.org/10.1021/jacs.5c05124
J. Am. Chem. Soc. 2025, 147, 25407−25416

would be generated when H_2O loses electron to FEP during the CE process. In the metal salt solution with FEP, the pH value decreased by approximately 6.79% to 42.7% with ultrasonication under aerobic conditions, while a more pronounced reduction of 23.21% to 52% was observed under anaerobic conditions (Figure S19). Based on the experimental results, the reduction capacity of metal ions and the production of H^+ under aerobic conditions were significantly lower compared to those under anaerobic conditions. This is most likely due to the occurrence of the ORR, where oxygen could react with electrons and H^+ to generate H_2O_2 or H_2O, supporting the hypothesis that the ORR played a key role in the CE-Chemistry process. To further investigate this hypothesis, electron paramagnetic resonance (EPR) spectroscopy was also conducted to measure and compare the electron transfer under aerobic and anaerobic conditions. 2,2,6,6-Tetramethylpiperidine 1-oxyl (TEMPO), a paramagnetic electron scavenger, was used as a spin probe to capture the electrons during the EPR analysis. Upon reduction to TEMPOH, TEMPO lost its paramagnetic properties, resulting in a decrease in the EPR signal. It was found from Figure 2c that the EPR signal of TEMPO during ultrasonication in the presence of FEP significantly decreased compared to that in the absence of FEP, indicating that the role of FEP was to enhance the electron transfer in CE. Besides, the reduction rate of TEMPO to TEMPOH was further promoted in CE-Chemistry with Ar gas, indicating that more electrons existed under anaerobic conditions. These findings unequivocally demonstrate that oxygen actively competes for electrons in the reduction reaction of CE-Chemistry under aerobic conditions.

Consequently, the design and regulation of CE-Chemistry systems must rigorously account for the influence of the ORR under ambient atmospheric conditions. Specifically, the SEPs of the $2e^-$ ORR (E^0 = 0.695 V vs NHE) and the $4e^-$ ORR (E^0 = 1.229 V vs NHE) provide critical benchmarks for modulating the CE-Chemistry reaction. Within the potential range defined by the $2e^-$ ORR (E^0 = 0.695 V vs NHE) and the $4e^-$ ORR (E^0 = 1.229 V vs NHE), the reduction of metals in CE-Chemistry was distinctly observed. In contrast, reductions in $K_3[Fe(CN)_6]$ and $CuSO_4$ were scarcely detectable below this range. Oxidation in CE-Chemistry appeared more readily achievable when the SEP of the reactant was below E^0= 0.695 V vs NHE, as illustrated by the oxidation of $K_4[Fe(CN)_6]$ to $K_3[Fe(CN)_6]$. This phenomenon may be attributed to the oxidative action of H_2O_2, generated via the $2e^-$ ORR, which enhanced oxidation within the reaction system. Furthermore, $^{\bullet}OH$ radicals, produced through electron loss from water molecules, likely contributed to the oxidation processes in CE-Chemistry.

Furthermore, the CE characteristics can be effectively modulated by adjusting the mechanical input, specifically the duration and power of ultrasonication, which determine the frequency and intensity of contact-separation events at the solid−liquid interface, thereby impacting the overall reaction outcome. As shown in Figure S20, increasing either the ultrasonic duration or the power results in a greater extent of $[AuCl_4]^-$ reduction, demonstrating a clear correlation between mechanical energy input and the efficiency of CE-driven redox reactions. Interestingly, the reduction rate decreased with increasing temperature, indicating a nonclassical mechanism despite exhibiting Arrhenius-type temperature dependence. This anomalous trend stems from the interfacial nature of CE-Chemistry: elevated temperatures enhance ionic mobility, leading to stronger electrical double layer (EDL) screening that suppresses interfacial electron transfer. Fitting the first-order kinetics to an Arrhenius plot yielded an apparent activation energy of −18.57 kJ mol^{-1} (Figure S21, inset).

CH_3OH Oxidation to HCHO through CE-Chemistry. Building upon these redox reactions, this approach may unveil novel pathways in CE-Chemistry, thereby broadening our understanding of the dualistic Janus behavior. By judiciously selecting dielectric materials and solvents, the intrinsic properties of CE can be tailored, facilitating control over reaction selectivity and efficiency, as exemplified by the conversion of CH_3OH to HCHO. The catalytic oxidation of CH_3OH to produce HCHO is a critical chemical process with significant industrial applications.[28,29] HCHO is a high-value chemical widely utilized in the production of resins, synthetic fibers, and adhesives.[30] Moreover, it plays a pivotal role as an intermediate in the conversion of carbon dioxide into starch,[31] with its yield directly influencing the efficiency of subsequent reactions. Traditional thermal catalytic methods for producing HCHO typically require high temperatures and pressures, which result in significant energy consumption and potential catalyst deactivation due to sintering or coking.[32] In contrast, electrocatalytic production of HCHO operates under milder conditions, offering reduced energy consumption and enhanced environmental sustainability.[33] However, this process is contingent upon an external power supply, and attaining high current densities remains a significant challenge, frequently resulting in constrained reaction efficiency and selectivity. In this study, CE-Chemistry was employed for the first time to directly catalyze the oxidation of CH_3OH to produce HCHO, achieving conversion without noble metal catalysts, thus significantly reducing energy consumption and costs.

The oxidation of CH_3OH was carried out in a beaker in an ambient environment. In this experiment, 20 mg of FEP was added to 50 mL of DI water and CH_3OH mixture, and the beaker was placed in an ultrasonic bath (40 kHz, 120 W) for sonication. The amount of HCHO was assessed under varying volume ratios of CH_3OH to H_2O. The acetylacetone colorimetric method was utilized to quantify the amount of HCHO produced by CE-Chemistry.[34] Specifically, HCHO reacted with acetylacetone and ammonia in a coordination reaction,[35] forming a stable yellow complex with a characteristic UV−vis absorption peak at 413 nm, the intensity of which exhibited a linear relationship with the HCHO amount. The detection mechanism of the acetylacetone colorimetric method, along with the corresponding calibration curve for the quantification of HCHO, is illustrated in Figures S22 and S23. As shown in Figure S24, the production rate of HCHO increased proportionally with the volume ratio of CH_3OH to H_2O in the presence of FEP, underscoring the pivotal role of water in contact with FEP in facilitating CE-Chemistry. The production rate of HCHO reached up to 2480 μmol g^{-1} h^{-1} at a volume ratio of CH_3OH to H_2O of 1:50. To further investigate the CE effect between water and FEP during CH_3OH oxidation, EPR spectroscopy was employed to detect the key intermediates involved in the CE-Chemistry process. As shown in Figure S25, quadruplet DMPO-$^{\bullet}OH$ characteristic peaks were observed in the aqueous system, suggesting the generation of $^{\bullet}OH$ during CE between water and FEP. The highly oxidative $^{\bullet}OH$ can oxidize CH_3OH to HCHO. This reaction mechanism has been reported in the relevant literature.[36,37] Therefore, the oxidation mechanism of

https://doi.org/10.1021/jacs.5c05124
J. Am. Chem. Soc. 2025, 147, 25407−25416

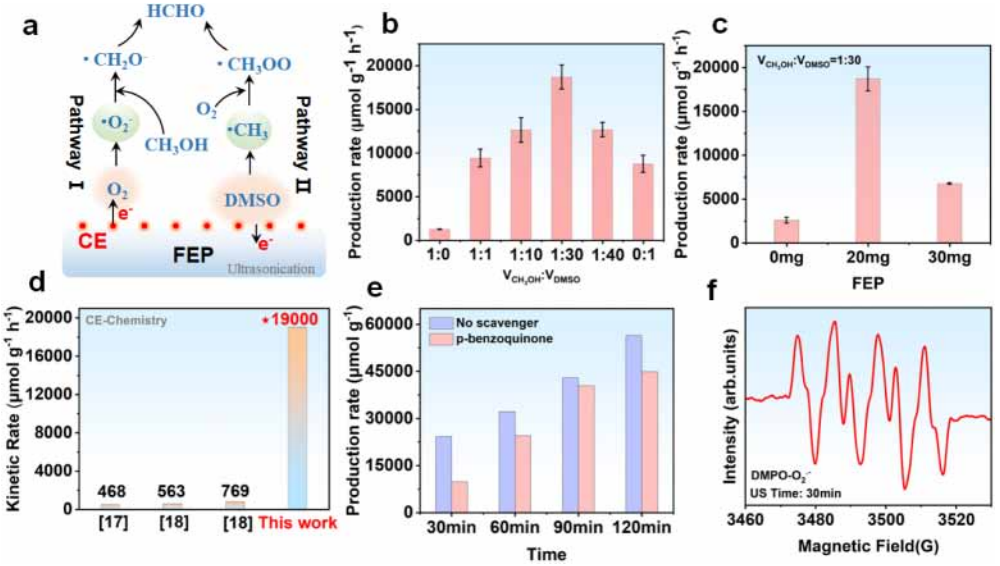

Figure 3. CH_3OH oxidation to HCHO through CE-Chemistry. (a) Schematic diagram of the oxidation of CH_3OH to HCHO via CE-Chemistry in DMSO. (b) Yield of HCHO at different volume ratios of CH_3OH and DMSO. (c) The production rate of HCHO at varying FEP mass. (d) Chart comparing the kinetic rate of recently reported CEC for the production rate of HCHO to the present work.[17,18] (e) Evolution of HCHO yield in the presence of *p*-benzoquinone radical scavengers. (f) Detection by EPR of DMPO-$^{\bullet}O_2^-$ under nonaqueous solution condition.

CH_3OH via CE-Chemistry in the aqueous system might follow these pathways: water molecules lose electrons to FEP during the CE process, forming water radical cations (eq 1). These cations are converted into hydrated cations and $^{\bullet}OH$ (eq 2). CH_3OH reacted with $^{\bullet}OH$ to form $HOCH_2OH$ (eqs 3 and 4). Subsequently, $HOCH_2OH$ underwent dehydration to produce HCHO (eq 5).

$$H_2O \rightarrow e^- + H_2O^{\bullet+} \quad (1)$$

$$H_2O^{\bullet+} + H_2O \rightarrow H_3O^+ + {}^{\bullet}OH \quad (2)$$

$$CH_3OH + {}^{\bullet}OH \rightarrow {}^{\bullet}CH_2OH + H_2O \quad (3)$$

$$^{\bullet}CH_2OH + {}^{\bullet}OH \rightarrow HOCH_2OH \quad (4)$$

$$HOCH_2OH \rightarrow HCHO + H_2O \quad (5)$$

It should be noted that the H^+ generated during CE in the aqueous system was likely adsorbed onto the negatively charged FEP surface, leading to the formation of an EDL[38,39] (Figure S26). This phenomenon inhibits subsequent interfacial electron transfer and hinders the dynamics of CE-Chemistry reactions.[40] The nonaqueous solvent DMSO has been reported to effectively mitigate the EDL screening effect[41] and has been widely utilized as an organic medium for electrosynthesis.[42] Therefore, it may enhance the reaction efficiency of HCHO in the CE-Chemistry system. Furthermore, the propensity of DMSO to generate methyl radicals ($^{\bullet}CH_3$)[41] upon contact with FEP likely played a role in enhancing HCHO production (Figure 3a). The inherent ability of DMSO to produce $^{\bullet}CH_3$ radicals under these conditions further contributed substantially to the overall yield of HCHO. This highlighted the flexibility and controllability of CE-Chemistry through the regulation of radical types by selecting the appropriate solvents. Moreover, the generation of $^{\bullet}O_2^-$ in the nonaqueous system, where O_2 accepts electrons from the negatively charged FEP, further facilitated the oxidation of CH_3OH to HCHO. A stepwise mechanism of oxidation in two different solvent systems is depicted in Figure S27 to clarify the proposed reaction pathways. The pivotal role of FEP in enhancing CE-driven chemical reactivity is demonstrated in Figure S28, where only a minor amount of HCHO is generated under ultrasonic treatment without FEP, in stark contrast to the significantly higher yield observed when FEP is present under identical conditions. This underscores FEP's critical role in facilitating interfacial electron transfer during the CE process, thereby improving reaction efficiency and enabling high HCHO yield. Furthermore, the dependence of HCHO generation on ultrasonication time (Figure S29) suggests that sonication serves as an effective means to modulate the frequency and intensity of solid−liquid contact events, thereby tuning the extent of CE-induced chemical reactions.

In addition, the production rate of HCHO in mixed solutions with different volume ratios of CH_3OH: DMSO values was compared after ultrasonication in the presence of FEP (Figure 3b). The optimal ratio of 1:30 likely reflects a balance between maintaining sufficient methanol as the reactive substrate for HCHO production and leveraging DMSO's ability to suppress EDL formation and enhance interfacial electron transfer. In contrast, higher methanol content (ratios >1:30) lowers the dielectric constant of the mixture (methanol: ε = 33.3; DMSO: ε = 47.2) and promotes EDL formation due to methanol's protic nature,[43−46] thereby reducing CE-driven reaction efficiency. Comparison of solvent effects on HCHO generation under CE-driven reactions (Figure S30) shows that among solvents tested at a CH_3OH:solvent ratio of 1:30, DMSO yields the highest HCHO production, as indicated by the strongest absorbance at 413 nm. Water's lower performance is attributed to proton-induced EDL formation on the negatively charged FEP surface, which hinders interfacial electron transfer. Similarly, ethanol, a protic solvent with a low dielectric constant (ε = 25.3), promotes EDL formation and restricts electron transfer, resulting in negligible HCHO generation. Acetone, although aprotic, has an even lower dielectric constant (ε = 20.7) compared to that of DMSO, leading to less efficient CE-induced oxidation. A higher dielectric constant often correlates

https://doi.org/10.1021/jacs.5c05124
J. Am. Chem. Soc. 2025, 147, 25407−25416

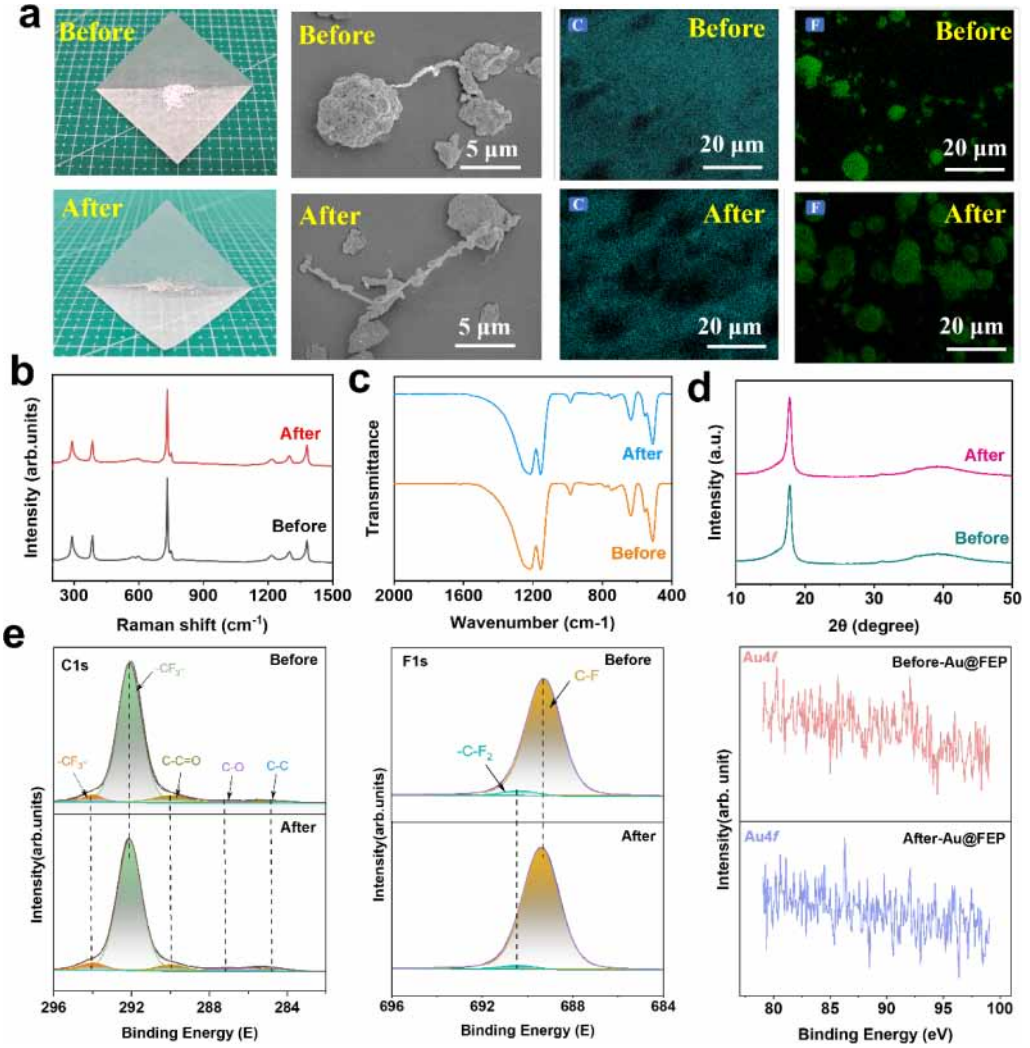

Figure 4. Characterization of FEP before and after CE-Chemistry. (a) Morphological characterization and EDX analysis of FEP before and after reaction. Raman spectra, FTIR spectra, and XRD spectra of the FEP before and after the CE-Chemistry reaction (b–d). (e) C 1s, F 1s, and Au 4f XPS spectra of FEP before and after the CE-Chemistry reaction.

with greater effective electronegativity, enhancing charge stabilization and interfacial electron transfer. DMSO's superior performance might arise from its relatively high dielectric constant (ε = 47.2) and aprotic nature, which minimize EDL screening and stabilize charge-separated states. This promotes the generation of $^{\bullet}CH_3$ radicals that drive HCHO formation, making it the most effective solvent for promoting CE-induced oxidation to HCHO.

In addition, the production rate of HCHO generated in the mixing solution with a volume ratio of CH_3OH: DMSO = 1:30 under varying masses of FEP was compared. As shown in Figure 3c, increasing the mass of FEP to 30 mg resulted in a reduction in the HCHO yield. This reduction likely stems from excessive FEP limiting effective reaction sites, resulting in insufficient contact and separation, ultimately reducing the HCHO yield.[18] The highest production rate of HCHO (19000 μmol g^{-1} h^{-1}) was achieved in the mixing solution with a volume ratio of CH_3OH: DMSO = 1:30 in the presence of 20 mg of FEP. To the best of our knowledge, this was the first demonstration of achieving a high production rate of HCHO through the CE-Chemistry process. As shown in Figure 3d, the HCHO production rate achieved by the CE-Chemistry method is not only comparable to many photocatalysis methods under similar conditions but also approximately 25 times higher than the rate reported for previous CEC methods (Table S2). It holds promise as a sustainable, metal catalyst-free, cost-effective, and energy-efficient alternative to conventional methods.

To further reveal the formation mechanism of HCHO, *p*-benzoquinone was introduced as a scavenger for $^{\bullet}O_2^-$ into the CE-Chemistry system, reaching a final concentration of 1 mM. Compared with the control experiments, the production rate of HCHO was reduced by the introduction of *p*-benzoquinone (Figure 3e). This result demonstrated that $^{\bullet}O_2^-$ played an important role in the formation of HCHO. To verify the hypothesized production of $^{\bullet}O_2^-$, EPR was used to detect the spin trap adducts during the CE-Chemistry process. In Figure 3f, the sextuplet characteristic peak signal produced by the adducts formed from the reaction between 5,5-dimethyl-1-pyrroline *N*-oxide (DMPO) and $^{\bullet}O_2^-$ was detected in pure DMSO solution, namely DMPO-O_2^-, after 30 min of ultrasonication in the presence of FEP. Based on the experimental results, the generation of HCHO might be attributed to the oxidation of CH_3OH via $^{\bullet}O_2^-$, following reaction pathway I: Oxygen acquired electrons from the FEP surface to form $^{\bullet}O_2^-$ during the CE process (eq 6). This $^{\bullet}O_2^-$

https://doi.org/10.1021/jacs.5c05124
J. Am. Chem. Soc. 2025, 147, 25407−25416

then deprotonated $^{\bullet}OH$ in CH_3OH (eq 7), undergoing a two-step reaction to form HCHO (eqs 8 and 9).

Pathway I: Oxidation of CH_3OH

$$O_2 + e^- \rightarrow {}^{\bullet}O_2^- \quad (6)$$

$$CH_3OH + {}^{\bullet}O_2^- \rightarrow CH_3O^- + HO_2 \quad (7)$$

$$CH_3O^- + HO_2^{\bullet} \rightarrow {}^{\bullet}CH_2O^- + H_2O_2 \quad (8)$$

$$^{\bullet}CH_2O^- + O_2 \rightarrow HCHO + {}^{\bullet}O_2^- \quad (9)$$

Additionally, upon contact with FEP, DMSO generated an ion peak at m/z 161.0969 ($[DMPO{-}OOCH_3 + H]^+$), corresponding to the formation of DMPO-captured $^{\bullet}CH_3OO$, which was directly observed by high-performance liquid chromatography−mass spectrometry (HPLC-MS) (Figure S31). As DMSO was reported to generate $^{\bullet}CH_3$[41], it is plausible that HCHO formation might also proceed through reaction pathway II (Figure 3a). During the CE process, DMSO underwent electron transfer to generate $^{\bullet}CH_3$ (eq 10). These $^{\bullet}CH_3$ radicals reacted with oxygen to form the intermediate $^{\bullet}CH_3OO$ (eq 11), which subsequently underwent transformation reactions, ultimately yielding HCHO (eq 12). The possible reaction process of HCHO production in the CE-Chemistry process was as follows:

Pathway II: Conversion of DMSO

$$C_2H_6SO \rightarrow 2{}^{\bullet}CH_3 + SO \quad (10)$$

$$^{\bullet}CH_3 + O_2 \rightarrow {}^{\bullet}CH_3OO \quad (11)$$

$$2{}^{\bullet}CH_3OO \rightarrow HCHO + CH_3OH + O_2 \quad (12)$$

The oxidation of CH_3OH in this study demonstrated that the flexible selection of solvents not only regulated the types of radical generation but also provided a significant advantage in enhancing external-power-free chemical synthesis.

Stability of FEP in CE-Chemistry. Effects of ultrasonic treatment on the physical and chemical properties of the FEP nanoparticle surface in aqueous and nonaqueous systems were also investigated. The morphological characterization and elemental mapping of FEP before and after CE-Chemistry in the aqueous system are illustrated in Figure 4a. Surface observations and scanning electron microscopy (SEM) revealed no apparent changes in coloration and morphology. Elemental mapping analysis using EDX confirmed that the composition of FEP remained unchanged before and after the reaction. Figures S32 and S33 illustrate that both SEM and EDX analyses of FEP remained unchanged after the CE-Chemistry process in the nonaqueous system. Nanoparticle size analysis further demonstrated that the FEP exhibited a negligible decrease in diameter after the reaction in both aqueous and nonaqueous systems, with no decomposition observed (Figure S34). Additionally, spectroscopic analysis techniques were employed to provide more comprehensive insights into the FEP in the aqueous system. The skeletal vibration modes of FEP before and after the reaction were consistent in Raman spectroscopy (Figure 4b). Furthermore, in Fourier transform infrared spectroscopy (FTIR), the fingerprint region below 1500 cm^{-1} remained stable after the reaction (Figure 4c). X-ray diffraction spectroscopy (XRD) results also indicated no shift in diffraction peak positions before and after the reaction (Figure 4d). Similarly, the Raman spectroscopy, FTIR, and XRD spectroscopy of FEP did not change after the CE-Chemistry process in the nonaqueous system (Figure S35). The chemical state stability of FEP was further evaluated using X-ray photoelectron spectroscopy (XPS) in the aqueous system. The C 1s and F 1s spectra of FEP are shown in Figure 4e. Neither shift in the binding energies of the original peaks nor the formation of new peaks was observed after the reaction. Meanwhile, analysis of the Au 4f spectra at the surface of FEP revealed no bonding between the FEP and gold atoms. These results confirmed that the chemically inert FEP served as catalysts for the reduction of metal ions during the reaction. The chemical state of FEP before and after CE-Chemistry was also analyzed by XPS in the nonaqueous system. The C 1s and F 1s spectra are shown in Figure S36. No shifts in the original peaks were observed, and no new peaks formed on the surface of the FEP. Furthermore, we assessed the total organic carbon (TOC) content of the aqueous system before and after the CE-Chemistry reaction to investigate possible degradation or side reactions. As shown in Figure S37, the negligible change in TOC levels confirms the chemical stability of FEP under the experimental conditions. This stability likely arises because, in CE-Chemistry, the generation of radicals and electron transfer are driven by the triboelectric field at the solid−liquid interface induced by CE, with the dielectric material itself not directly participating in chemical reactions. The above results showed that FEP maintained high chemical inertness and stability before and after the CE-Chemistry reaction in both aqueous and nonaqueous systems.

CONCLUSION

In this study, the redox reaction tendencies in ultrasound-assisted Janus CE-Chemistry are systematically unified for the first time by SEPs, highlighting the pivotal role of the $2e^-$ ORR in the CE-Chemistry process. The reductions of $[AuCl_4]^-$, Pd^{2+}, $[PtCl_4]^{2-}$, Ag^+, Rh^{3+}, and Ir^{3+} were successfully driven by electron transfer from the dielectric surface at the CE interface between water and FEP, as further validated by DFT simulations. Comparison of the SEPs of various metal ions revealed that reduction reactions predominantly occur when the SEPs exceed 0.695 V, with a marked decrease in reduction tendency when the SEPs are below this threshold. Notably, the amount of metal ion reduction under anaerobic conditions was significantly higher than that under aerobic conditions. Unveiling Janus chemical processes in CE-Chemistry through ORR paves the way for expanding its application across diverse catalytic and reaction systems. Furthermore, this study achieved the oxidation of CH_3OH to HCHO in both aqueous and nonaqueous systems via CE-Chemistry for the first time. The exploration of nonaqueous solvents demonstrated their efficiency in mitigating the EDL effect and regulating radical types, thereby enhancing reaction efficiency. Remarkably, under DMSO solvent conditions, the production rate of HCHO achieved through the synergistic interaction between DMSO and CH_3OH is approximately 25 times greater than that reported in previous CEC aqueous systems. These findings highlighted the critical role of solvent selection in optimizing reaction efficiency and established CE-Chemistry as a transformative paradigm for chemical reactions. This work provided profound theoretical insights into triboelectric-charge-regulated chemical processes. Ultimately, integrating CE-Chemistry with traditional electrochemistry might further revolutionize catalysis, providing a versatile, eco-friendly, and cost-effective solution for diverse industrial applications.

https://doi.org/10.1021/jacs.5c05124
J. Am. Chem. Soc. 2025, 147, 25407−25416

■ ASSOCIATED CONTENT

Data Availability Statement

The authors declare that all the data that support the findings of this study are available within the article and Supporting Information. Correspondence and requests for materials should be addressed to Hanbin Liu, Zhonglin Wang, or Di Wei.

Supporting Information

The Supporting Information is available free of charge at https://pubs.acs.org/doi/10.1021/jacs.5c05124.

Experimental section **1**; materials **2**; reagents **3**; sample preparation **4**; quantitative characterization of hydrogen peroxide (H_2O_2) **5**; chronoamperometry measurement **6**; quantitative characterization of formaldehyde (HCHO) **7**; electron paramagnetic resonance spectroscopy **8**; sample characterization **9**; effect of temperature on the activation energy of a reaction **10**; simulation methods **11**; results and discussion **12**; references **13** (PDF)

■ AUTHOR INFORMATION

Corresponding Authors

Hanbin Liu − *College of Bioresource Chemical and Materials Engineering, Shaanxi Provincial Key Laboratory of Papermaking Technology and Specialty Paper Development, Shaanxi University of Science & Technology, Xi'an 710021, P. R. China;* orcid.org/0000-0002-2141-796X; Email: liuhanbin@sust.edu.cn

Zhonglin Wang − *Beijing Institute of Nanoenergy and Nanosystems, Chinese Academy of Sciences, Beijing 101400, P. R. China; Georgia Institute of Technology, Atlanta, Georgia 30332-0245, United States*; Email: zlwang@binn.cas.cn

Di Wei − *Beijing Institute of Nanoenergy and Nanosystems, Chinese Academy of Sciences, Beijing 101400, P. R. China; Centre for Photonic Devices and Sensors, University of Cambridge, Cambridge CB3 0FA, U.K.;* orcid.org/0000-0003-2670-6362; Email: weidi@binn.cas.cn

Authors

Ting Gan − *Beijing Institute of Nanoenergy and Nanosystems, Chinese Academy of Sciences, Beijing 101400, P. R. China; College of Bioresource Chemical and Materials Engineering, Shaanxi Provincial Key Laboratory of Papermaking Technology and Specialty Paper Development, Shaanxi University of Science & Technology, Xi'an 710021, P. R. China*

Zhe Yang − *Beijing Institute of Nanoenergy and Nanosystems, Chinese Academy of Sciences, Beijing 101400, P. R. China; School of Nanoscience and Engineering, University of Chinese Academy of Sciences, Beijing 100049, P. R. China*

Shaoxin Li − *Beijing Institute of Nanoenergy and Nanosystems, Chinese Academy of Sciences, Beijing 101400, P. R. China; School of Nanoscience and Engineering, University of Chinese Academy of Sciences, Beijing 100049, P. R. China*

Han Qian − *Beijing Institute of Nanoenergy and Nanosystems, Chinese Academy of Sciences, Beijing 101400, P. R. China; School of Nanoscience and Engineering, University of Chinese Academy of Sciences, Beijing 100049, P. R. China;* orcid.org/0009-0005-8692-2317

Zhijian Li − *College of Bioresource Chemical and Materials Engineering, Shaanxi Provincial Key Laboratory of Papermaking Technology and Specialty Paper Development, Shaanxi University of Science & Technology, Xi'an 710021, P. R. China*

Jiajin Liu − *Beijing Institute of Nanoenergy and Nanosystems, Chinese Academy of Sciences, Beijing 101400, P. R. China; School of Nanoscience and Engineering, University of Chinese Academy of Sciences, Beijing 100049, P. R. China*

Puguang Peng − *Beijing Institute of Nanoenergy and Nanosystems, Chinese Academy of Sciences, Beijing 101400, P. R. China; School of Nanoscience and Engineering, University of Chinese Academy of Sciences, Beijing 100049, P. R. China*

Jinbo Bai − *Université Paris-Saclay, CentraleSupélec, ENS Paris-Saclay, CNRS, LMPS - Laboratoire de Mécanique Paris-Saclay, Gif-sur-Yvette 91190, France*

Complete contact information is available at: https://pubs.acs.org/10.1021/jacs.5c05124

Author Contributions

[▽]T.G., Z.Y., S.L., and H.Q. contributed equally to this work.

Notes

The authors declare no competing financial interest.

■ ACKNOWLEDGMENTS

This work was supported by the National Natural Science Foundation (grant number 22479016).

■ REFERENCES

(1) Yoshikawa, S.; Shimada, A. Reaction Mechanism of Cytochrome c Oxidase. *Chem. Rev.* **2015**, *115*, 1936−1989.

(2) Wikström, M.; Krab, K.; Sharma, V. Oxygen Activation and Energy Conservation by Cytochrome c Oxidase. *Chem. Rev.* **2018**, *118*, 2469−2490.

(3) Kishi, S.; Nagasu, H.; Kidokoro, K.; Kashihara, N. Oxidative stress and the role of redox signalling in chronic kidney disease. *Nat. Rev. Nephrol.* **2024**, *20*, 101−119.

(4) He, H.; Wu, X.; Zhu, J.; Lin, M.; Lv, Y.; Xian, H.; Yang, Y.; Lin, X.; Li, S.; Li, Y. A mineral-based origin of Earth's initial hydrogen peroxide and molecular oxygen. *Proc. Natl. Acad. Sci. U. S. A.* **2023**, *120*, No. e2221984120.

(5) Lee, J. K.; et al. Condensing water vapor to droplets generates hydrogen peroxide. *Proc. Natl. Acad. Sci. U. S. A.* **2020**, *117*, 30934−30941.

(6) Mehrgardi, M. A.; Mofidfar, M.; Zare, R. N. Sprayed Water Microdroplets Are Able to Generate Hydrogen Peroxide Spontaneously. *J. Am. Chem. Soc.* **2022**, *144*, 7606−7609.

(7) Lee, J. K.; et al. Spontaneous generation of hydrogen peroxide from aqueous microdroplets. *Proc. Natl. Acad. Sci. U. S. A.* **2019**, *116*, 19294−19298.

(8) Zhao, J.; Zhang, X.; Xu, J.; Tang, W.; Lin Wang, Z.; Ru Fan, F. Contact-electro-catalysis for Direct Synthesis of H_2O_2 under Ambient Conditions. *Angew. Chem., Int. Ed.* **2023**, *62*, No. e202300604.

(9) Berbille, A.; Li, X.-F.; Su, Y.; Li, S.; Zhao, X.; Zhu, L.; Wang, Z. L. Mechanism for Generating H_2O_2 at Water-Solid Interface by Contact-Electrification. *Adv. Mater.* **2023**, *35*, 2304387.

(10) Wang, Z.; Dong, X.; Tang, W.; Wang, Z. L. Contact-electro-catalysis (CEC). *Chem. Soc. Rev.* **2024**, *53*, 4349−4373.

(11) Wang, Z. L.; Wang, A. C. On the origin of contact-electrification. *Mater. Today* **2019**, *30*, 34−51.

(12) Wang, Z.; Berbille, A.; Feng, Y.; Li, S.; Zhu, L.; Tang, W.; Wang, Z. L. Contact-electro-catalysis for the degradation of organic pollutants using pristine dielectric powders. *Nat. Commun.* **2022**, *13*, 130.

(13) Wang, Z.; Dong, X.; Li, X.-F.; Feng, Y.; Li, S.; Tang, W.; Wang, Z. L. A contact-electro-catalysis process for producing reactive oxygen species by ball milling of triboelectric materials. *Nat. Commun.* **2024**, *15*, 757.
(14) Li, H.; et al. A contact-electro-catalytic cathode recycling method for spent lithium-ion batteries. *Nat. Energy* **2023**, *8*, 1137−1144.
(15) Li, S.; Zhang, Z.; Peng, P.; Li, X.; Wang, Z. L.; Wei, D. A green approach to induce and steer chemical reactions using inert solid dielectrics. *Nano Energy* **2024**, *122*, 109286.
(16) Li, S.; Liu, J.; Wang, Z. L.; Wei, D. Mechano-driven chemical reactions. *Green Energy Environ.* **2025**, *10*, 937−966.
(17) Jia, T.; Wang, W.; Zhang, C.; Zhang, L.; Wang, W. Polydopamine-Mediated Contact-Electro-Catalysis for Efficient Partial Oxidation of Methane. *Angew. Chem., Int. Ed.* **2025**, *64*, No. e202413343.
(18) Li, W.; Sun, J.; Wang, M.; Xu, J.; Wang, Y.; Yang, L.; Yan, R.; He, H.; Wang, S.; Deng, W.-Q.; et al. Contact-Electro-Catalysis for Direct Oxidation of Methane under Ambient Conditions. *Angew. Chem., Int. Ed.* **2024**, *63*, No. e202403114.
(19) Han, C.; et al. Selective Cleavage of Chemical Bonds in Targeted Intermediates for Highly Selective Photooxidation of Methane to Methanol. *J. Am. Chem. Soc.* **2023**, *145*, 8609−8620.
(20) Cao, Y.; Yu, W.; Han, C.; Yang, Y.; Rao, Z.; Guo, R.; Dong, F.; Zhang, R.; Zhou, Y.; et al. Methane Photooxidation with Nearly 100% Selectivity Towards Oxygenates: Proton Rebound Ensures the Regeneration of Methanol. *Angew. Chem., Int. Ed.* **2023**, *62*, No. e202302196.
(21) Su, H.; Han, J.-T.; Miao, B.; Salehi, M.; Li, C.-J. Photosynthesis of CH_3OH via oxygen-atom-grafting from CO_2 to CH_4 enabled by AuPd/GaN. *Nat. Commun.* **2024**, *15*, 6435.
(22) Jia, T.; et al. An efficient strategy for the partial oxidation of methane into methanol over POM-immobilized MOF catalysts under ambient conditions. *Appl. Catal., B* **2024**, *340*, 123168.
(23) Zhou, H.; Chen, F.; Liu, D.; Qin, X.; Jing, Y.; Zhong, C.; Shi, R.; Liu, Y.; Zhang, J.; Zhu, Y.; et al. Boosting Reactive Oxygen Species Formation Over Pd and VO_δ Co-Modified TiO_2 for Methane Oxidation into Valuable Oxygenates. *Small* **2024**, *20*, 2311355.
(24) Zhou, K.; et al. Deciphering the Kinetics of Spontaneous Generation of H_2O_2 in Individual Water Microdroplets. *J. Am. Chem. Soc.* **2024**, *146*, 2445−2451.
(25) Su, Y.; Berbille, A.; Li, X.-F.; Zhang, J.; PourhosseiniAsl, M.; Li, H.; Liu, Z.; Li, S.; Liu, J.; Zhu, L.; et al. Reduction of precious metal ions in aqueous solutions by contact-electro-catalysis. *Nat. Commun.* **2024**, *15*, 4196.
(26) Suslick, K. S. Mechanochemistry and sonochemistry: Concluding remarks. *Faraday Discuss* **2014**, *170*, 411−422.
(27) Vanysek, P.Electrochemical seriesCRC pressBoca Raton, FL2000*CRC handbook of chemistry and physics*88−33
(28) Sam, B.; Breit, B.; Krische, M. J. Paraformaldehyde and Methanol as C1 Feedstocks in Metal-Catalyzed C-C Couplings of π-Unsaturated Reactants: Beyond Hydroformylation. *Angew. Chem., Int. Ed.* **2015**, *54*, 3267−3274.
(29) Bahmanpour, A. M.; Hoadley, A.; Tanksale, A. Formaldehyde production via hydrogenation of carbon monoxide in the aqueous phase. *Green Chem.* **2015**, *17*, 3500−3507.
(30) Tian, W.; et al. Recent progress of biomass in conventional wood adhesives: A review. *Green Chem.* **2023**, *25*, 10304−10337.
(31) Cai, T.; et al. Cell-free chemoenzymatic starch synthesis from carbon dioxide. *Science* **2021**, *373*, 1523−1527.
(32) van Steen, E.; Guo, J.; Hytoolakhan Lal Mahomed, N.; Leteba, G. M.; Mahlaba, S. V. L. S. Selective, Aerobic Oxidation of Methane to Formaldehyde over Platinum - a Perspective. *ChemCatchem* **2023**, *15*, No. e202201238.
(33) Bin Yeo, J.; Ho Jang, J.; In Jo, Y.; Woo Koo, J.; Tae Nam, K. Paired Electrosynthesis of Formaldehyde Derivatives from CO_2 Reduction and Methanol Oxidation. *Angew. Chem., Int. Ed.* **2024**, *63*, No. e202316020.
(34) Chen, J.; Stepanovic, S.; Draksharapu, A.; Gruden, M.; Browne, W. R. A Non-Heme Iron Photocatalyst for Light-Driven Aerobic Oxidation of Methanol. *Angew. Chem., Int. Ed.* **2018**, *57*, 3207−3211.
(35) Wei, S.; et al. Aerobic oxidation of methane to formaldehyde mediated by crystal-O over gold modified tungsten trioxide via photocatalysis. *Appl. Catal., B* **2021**, *283*, 119661.
(36) Wang, C.-Y.; Rabani, J.; Bahnemann, D. W.; Dohrmann, J. K. Photonic efficiency and quantum yield of formaldehyde formation from methanol in the presence of various TiO_2 photocatalysts. *J. Photochem. Photobiol., A* **2002**, *148*, 169−176.
(37) Zhang, R.; et al. Direct Photocatalytic Methane Oxidation to Formaldehyde by N Doping Co-Decorated Mixed Crystal TiO_2. *ACS Nano* **2024**, *18*, 12994−13005.
(38) Li, X.; Li, R.; Li, S.; Wang, Z. L.; Wei, D. Triboiontronics with temporal control of electrical double layer formation. *Nat. Commun.* **2024**, *15*, 6182.
(39) Li, X.; Wang, Z. L.; Wei, D. Scavenging Energy and Information through Dynamically Regulating the Electrical Double Layer. *Adv. Funct. Mater.* **2024**, *34*, 2405520.
(40) Li, X.; et al. Triboiontronics for efficient energy and information flow. *Matter* **2023**, *6*, 3912−3926.
(41) Liu, J.; et al. Nonaqueous Contact-Electro-Chemistry via Triboelectric Charge. *J. Am. Chem. Soc.* **2024**, *146*, 31574−31584.
(42) Wei, D.; et al. Electrosynthesis and characterisation of poly(N-methylaniline) in organic solvents. *J. Electroanal. Chem.* **2005**, *575*, 19−26.
(43) Shock, C. J.; Stevens, M. J.; Frischknecht, A. L.; Nakamura, I. Molecular dynamics simulations of the dielectric constants of salt-free and salt-doped polar solvents. *J. Chem. Phys.* **2023**, *159*, 134507.
(44) Kohns, M. Molecular simulation study of dielectric constants of pure fluids and mixtures. *Fluid Phase Equilib.* **2020**, *506*, 112393.
(45) Mohsen-Nia, M.; Amiri, H.; Jazi, B. Dielectric constants of water, methanol, ethanol, butanol and acetone: Measurement and computational study. *J. Solution Chem.* **2010**, *39*, 701−708.
(46) MacGregor, W. S. The chemical and physical properties of DMSO. *Ann. N. Y. Acad. Sci.* **1967**, *141*, 3−12.

https://doi.org/10.1021/jacs.5c05124
J. Am. Chem. Soc. 2025, 147, 25407−25416